A SUPPLEMENTARY

A.1 Visualization Efficacy Comparison With More Baselines

A.1.1 Compare with PLA. One simple difference between our work and PLA [b] is that we use joint segments of sampled points for visualization while [b] uses disjoint segments for lossy compression. When disjoint segments are used for visualization, visual artifacts are produced from the connected lines of disjoint ends.

In essence, we target a different goal from PLA. PLA [b] uses RMSE to measure data fidelity, i.e., reconstruction accuracy in the data space. We uses SSIM [19, 25, 35] to measure visual fidelity, i.e., pixel-level or ideally perceptual-level, similarity in the image space. We provide in Section A.3 a detailed formula for the widely used SSIM metric, which accounts for variations in luminance, contrast, and structural components that are valued by the "human visual system". The fundamental difference between these two metrics is that RMSE operates in the t-v data space, while SSIM operates in the x-y image space. The two spaces have different resolutions and scales. In terms of resolution, certain discrepancies in the data domain may not be visible at pixel resolution, and on the other hand, tolerable errors in the data domain may be visually apparent. In terms of scales, varying scales for the time and value axes are used in line charts [A]. Usually, a small unit on the time axis represents a larger range or duration than the same unit on the value axis. Hence visible pixel errors along the value dimension may be underestimated by the data-space metrics. Our empirical experiments in Section A.1.3 confirm these differences.

A.1.2 Compare with Cartographic Simplification. Our goal is closer to that of cartographic simplification [f], because we all recognize humans as the ultimate consumers of approximation. Hence we prioritize understanding how humans perceive images. For example, Attneave [13][f] identified high curvature points as perceptually important. In contrast, dimensionality reduction techniques for similarity search often focus on lower bounding the Euclidean distance, potentially sacrificing visually significant points due to a smoothing effect [B]. However, there are still differences between our goal and that of [f]. While [f] is in the field of general cartographic simplification, our work focuses more on the specific domain of time series line charts, where different scales for the time and value axes need to be considered.

A.1.3 Empirical Comparison. we add three more methods into comparison, which are Sim-Piece [e], reuwi [29], and visval [33]. Sim-Piece is one of the most recent works on Piecewise Linear Approximation (PLA). It exploits the similarities of PLA segments to achieve compact representations in the field of lossy compression. Reuwi and visval are two classical methods in the field of cartographic simplification. Reuwi uses a point-to-line perpendicular distance threshold in the data space to sequentially segment time series. Visval proposes a bottom-up method to generalize lines by repeatedly eliminating the point with the smallest triangle area.

Figure 15 shows the SSIM comparison results. The visualizations of the sample data under $m = 320$ is shown in Figure 16. The first row, colored in green, presents the line charts of the original time series from four datasets. Each subsequent row represents a different sampling method, with the SSIM metric displayed above to evaluate its similarity to the original line chart, considered as the ground truth. Within each column (i.e., for each dataset), the top four methods with the highest SSIM values are highlighted using blue solid-line rectangles. Additionally, visual defects of different sampling algorithms are emphasized with red dashed-line rectangles.

As shown in the last three rows of Figure 16, the red dashed rectangles highlight the visual defects of the three added baselines. For Sim-Piece, it generates visual artifacts that do not exist in the data but are produced by connecting lines with disjoint ends. Besides, some regions with fewer segments succeed in keeping data fidelity, but fails to maintain visual fidelity (i.e. looking sparse). For reuwi, it misses many vertical spikes because pixel errors in the value direction is underestimated by the data-space perpendicular distance metric. For visval, it does not have the disadvantage of the previous two methods that an area is sparsely represented by a segment, but it has the disadvantage of missing sharp spikes due to their small triangle areas. In contrast, our proposed ILTS consistently ranks among the top four in terms of visual fidelity.

[b] Themis Palpanas, Time Series Summarization Using User-Defined Amnesic Functions. IEEE Trans. Knowl. Data Eng. 20(7): 992-1006 (2008)

[e] Kitsios, Panagiotis Liakos, Sim-Piece: Highly Accurate Piecewise Linear Approximation through Similar Segment Merging. Proc. VLDB Endow. 16(8): 1910-1922 (2023)

[f] The awakening of Attneave's sleeping cat: identification of everyday objects on the basis of straight-line versions of outlines Joeri De Winter 1, Johan Wagemans

[A] Anshul Vikram Pandey, Katharina Rall, Margaret L. Satterthwaite, Oded Nov, and Enrico Bertini. 2015. How Deceptive are Deceptive Visualizations? An Empirical Analysis of Common Distortion Techniques. In Proceedings of the 33rd Annual ACM Conference on Human Factors in Computing Systems (CHI '15). Association for Computing Machinery, New York, NY, USA, 1469–1478. https://doi.org/10.1145/2702123.2702608

[B] Tak-chung Fu, Fu-lai Chung, Robert Luk, and Chak-man Ng. 2008. Representing financial time series based on data point importance. Eng. Appl. Artif. Intell. 21, 2 (March, 2008), 277–300. https://doi.org/10.1016/j.engappai.2007.04.009

A.2 System Architecture and Response Time Decomposition

This section illustrates our motivation to expedite in-database sampling queries.

A.2.1 Data Visualization System. A typical data visualization system is shown in Figure 17. Large-scale time series data are stored in the remote database. When a user requests an ad-hoc visualization of a time series, the visualization client sends an online query request to the database. The query executor of the database deals with metadata and data and sends the result data back to the client. Finally, the client renders the data on the screen.

A.2.2 Response Time Decomposition. The big data poses challenges to every aspect of the visualization system, including database querying, communicating, and rendering [21]. We experiment on

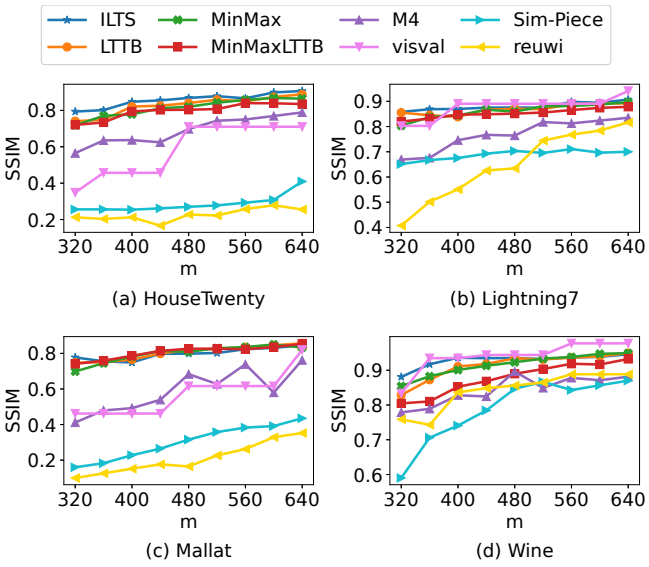

Figure 15: SSIM comparison experiments (Sim-Piece, reuwi, and visval baselines added)

the response time decomposition and the results are shown in Figure 18.

Rendering. The client rendering time refers to the duration taken by Python to execute `plt.plot(t,v)` function. It turns out that Python requires around 20 seconds to plot 300 million data points. Moreover, in our practical experience, Grafana dashboard, as another widely used visualization tool, encounters out-of-memory errors when attempting to visualize time series data exceeding 100 million points.

Querying. While in-memory similarity search queries [a] have demonstrated remarkable speed, we focus on queries within disk-based databases as illustrated in Figure 17. Firstly, the underlying physical storage of data challenges fast querying. Note that high concurrency data writes are common in IoT scenarios, where thousands of devices with millions of sensors continuously ingest data into the database. Buffered time series data are periodically flushed to disk once the memory threshold is reached. For instance, as shown in Figure 17, the time series "A" marked in green is stored as pages across dispersed disk locations within a file. While compaction strategies are used to periodically merge small pages into larger ones, the dispersed I/O remains unavoidable and substantially impact the query performance. Secondly, the upper-layer encapsulation step of the query result set is also time-consuming for large data volumes. Consequently, executing raw data queries in such disk-based databases is time consuming. In our experiments, the execution time of the raw data query for 300 million points reached 200 seconds.

Communicating. Communication is also challenged by big data. In our experiments, transferring 300 million data points from the remote database to the visualization client takes seven minutes. Moreover, when multiple clients are connected to the database for data transmission simultaneously, the number of clients the server can serve concurrently is limited due to bandwidth constraints [25].

A.2.3 Our Focus. Recently Plotly-resampler [32] proposes applying sampling in the frontend plotting software to address the slow rendering issues of big data. However, considering the large communication delays for big data transferred from the remote database, we believe that in-database sampling is essential. As shown in Figure 18, sampling queries such as LTTB can be employed instead of raw data queries to reduce data transfer and rendering time. Consequently, database query execution time becomes the bottleneck. Hence our work contributes to accelerating such in-database online sampling queries to further decrease the response time of visualization applications [28]. Specifically, we use precomputed convex hulls to accelerate online largest triangle sampling queries. Note that while a time series is stored as pages across various disk locations within a file, the metadata for these pages is stored contiguously at the end of the file, which is I/O friendly.

[a] https://www.cs.unm.edu/ mueen/FastestSimilaritySearch.html

A.3 SSIM Formula

Let X and Y denote the pixel matrices of two images with the same dimensions $w \times h$. A simple error measure of the two images is the Mean Squared Error, i.e., $MSE(X,Y) = \frac{1}{wh}\sum_{i=1}^{w}\sum_{j=1}^{h}(X_{ij}-Y_{ij})^2$. The Structural SIMilarity (SSIM) index [19, 25, 35] is further proposed to account for variations in luminance, contrast, and structural components that are valued by human perception. Formally,

$$SSIM(X,Y) = \frac{(2\mu_x\mu_y + C_1)(2\sigma_{xy} + C_2)}{(\mu_x^2 + \mu_y^2 + C_1)(\sigma_x^2 + \sigma_y^2 + C_2)},$$

where μ_x, μ_y are the average intensities for luminance comparison, σ_x^2, σ_y^2 are the variances for contrast comparison, σ_{xy} is the covariance of X and Y for structure comparison, and C_1, C_2 are small constants to stabilize division operations. SSIM yields a score within the range of -1 to 1, where values closer to 1 indicate higher visual similarity.

In practice, SSIM is computed within a local window (e.g., a 11×11 square window) that slides across the entire image. The overall image quality is determined by averaging these SSIM values obtained from all windows, a method known as Mean SSIM (MSSIM) [35]. Considering the prevalent white background in time series line charts, the OR-conv masking technique for SSIM [19] is introduced to effectively exclude the shared white background from comparison, enhancing the discriminability of the metric. In our experiments, we evaluate the visualization efficacy of sampling algorithms by calculating the masked SSIM between the original and the sampled line charts. The larger the SSIM value, the better the visual fidelity of the sampling algorithm.

Take Figure 19 as an example. Suppose that we sample eight points (i.e., $m = 8$) from an input time series of length $n = 600$ and render the line chart on a 6×10 canvas. The first column represents the original time series, and each subsequent column corresponds to a different sampling algorithm. The first row displays the time series in high resolution, and the second row shows the rendered line charts. The bottom row uses different colors to encode the pixel differences between the original (labeled as "ground truth") and sampled line charts. Green pixels indicate those unmarked in

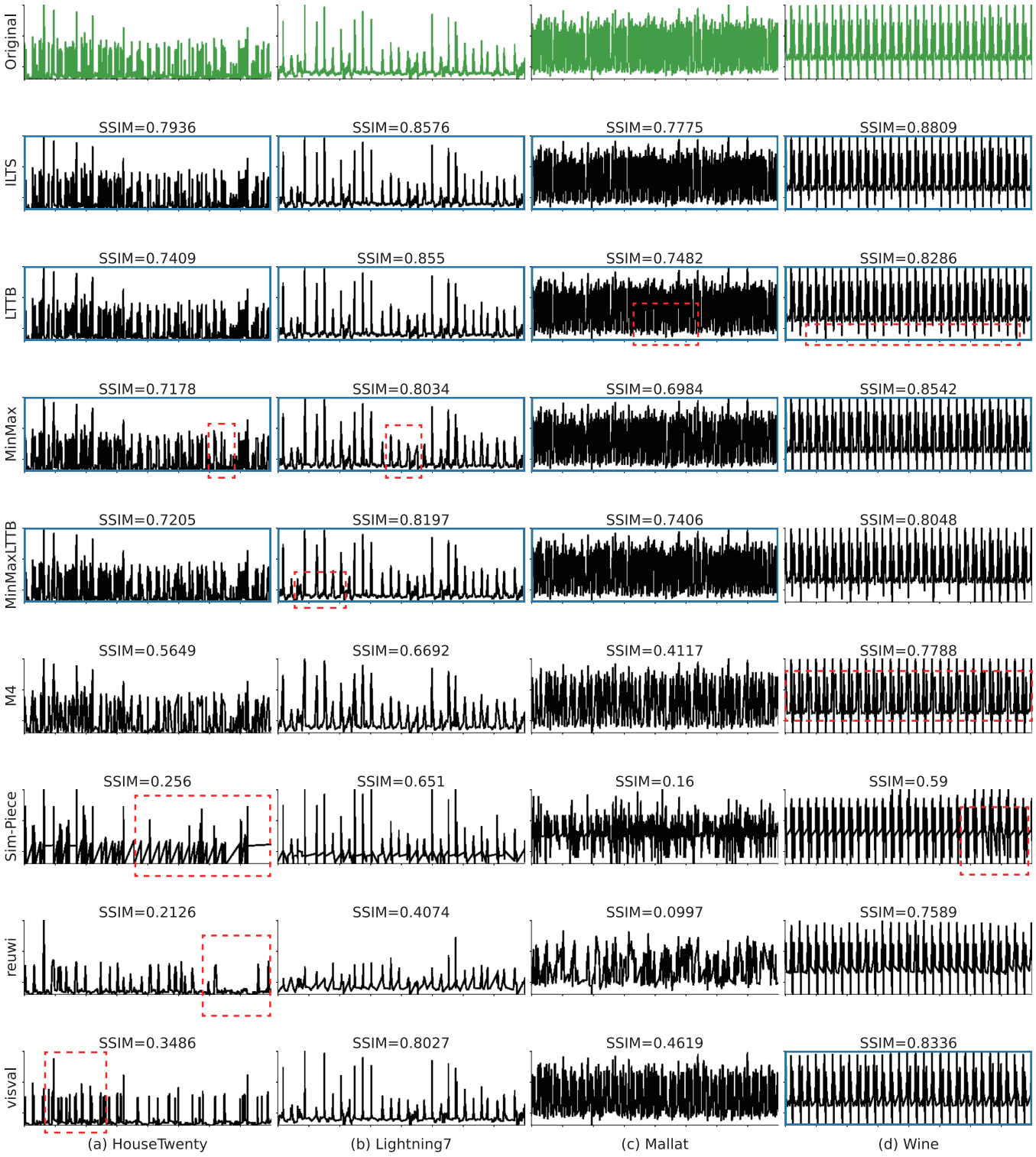

Figure 16: Visualizations of sample data. Blue solid-line rectangles highlight the top four methods with the highest SSIM values within each column. Red dashed-line rectangles emphasize the visual defects of different sampling algorithms.

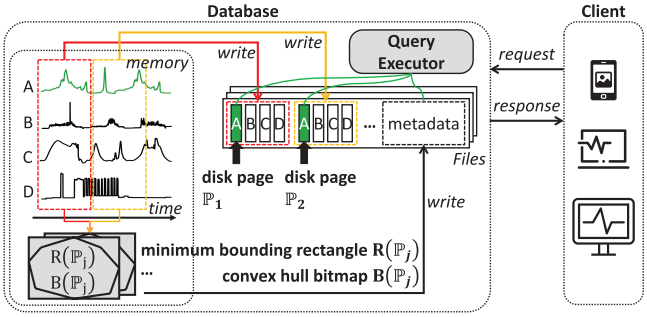

Figure 17: Architecture of a data visualization system with a disk-based remote database

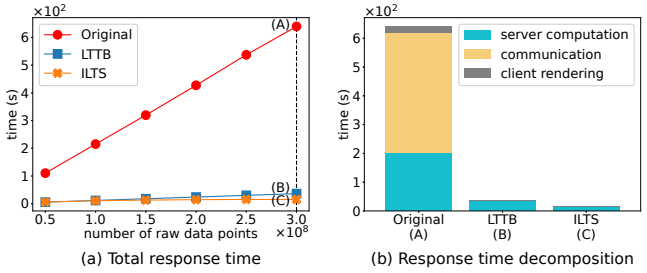

Figure 18: Cost of visualizing time series from a remote database

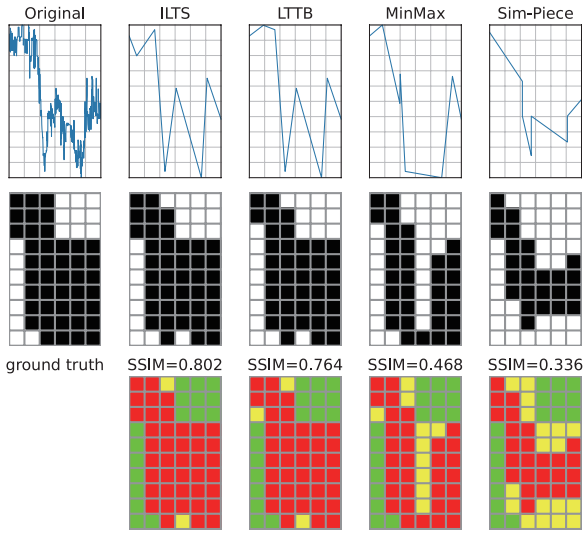

Figure 19: Example of SSIM on rasterized line charts

both images, red pixels indicate those marked in both images, and yellow pixels denote those marked in the original but missed in the sampled image. The SSIM results show that our proposed ILTS achieves the best visual fidelity.

A.4 Proof of Proposition 1

According to [31], the Largest-Triangle-Three-Buckets (LTTB) algorithm goes through buckets B_i from left to right (i.e., from $i = 2$ to $i = m - 1$) and works at three bucket at a time. It employs the selected point from the previous bucket and the average point of the next bucket as heuristic points. The algorithm then selects the point in the current bucket that forms the largest triangle area with these two heuristic points. It is important to note that LTTB does not directly output the average point of each bucket as the final sampled result. If the Iterative Largest Triangle Sampling (ILTS) algorithm is initiated using average points and iterated one step further, it will identify an identical set of points as LTTB, since both algorithms utilize the same heuristic points for selection from the same set of points. Therefore, we prove that LTTB is a special case of ILTS.

A.5 Time Complexity Analysis

Figure 17 gives an overview of the data write and read process. When the in-memory time series data are flushed to dispersed disk locations as pages, the metadata of these pages are retained in memory because metadata is much smaller than data. When a file is to be closed, the metadata are then written sequentially to the end of the file. During querying processing, the query executor first loads all metadata into memory and the minimum bounding rectangle (MBR) in the metadata is utilized to prune unnecessary pages (Section 4.3). For pages unpruned, I/Os are inevitable; however, we can leverage the convex hull bitmap metadata to fast search on the convex hull points, thereby reducing CPU costs (Section 4.2). The query cost can be modelled as follows.

$$T = T_M + \sum_{i=1}^{c} I_i * (T_D + k * T_P),$$

where

- T_M: the time cost of loading all relevant metadata into memory
- c: the total number of pages for the time series
- I_i: 0 if the i-th page is pruned by the MBR, 1 otherwise
- T_D: the time cost of loading one disk page into memory
- T_P: the time cost of traversing all points in a page
- k: a coefficient between [0,1], reflecting the proportion of searched convex hull points to the total number of points in the page

A.6 Avoid Redundant Computation

Algorithm 3 enhances Algorithm 1 by adding the redundancy removal logic as introduced in Section 3.2. Specifically, Line 9 shows that the condition when a bucket can reuse the sampling point from the previous iteration is met. $leftEq = true$ and $R_{i+1} = true$ means that its left and right adjacent latest sampled points remain unchanged in their last two iterations, respectively. Line 17 shows that the condition to exit the iteration is met, which occurs when all sampled points remain unchanged in their last two iterations.

A.7 Visualization Efficacy Comparison Using Other Initialization Mechanism

Referring to line 2 of Algorithm 1, the proposed ILTS can initialize by either random or average points in the buckets. We experiment

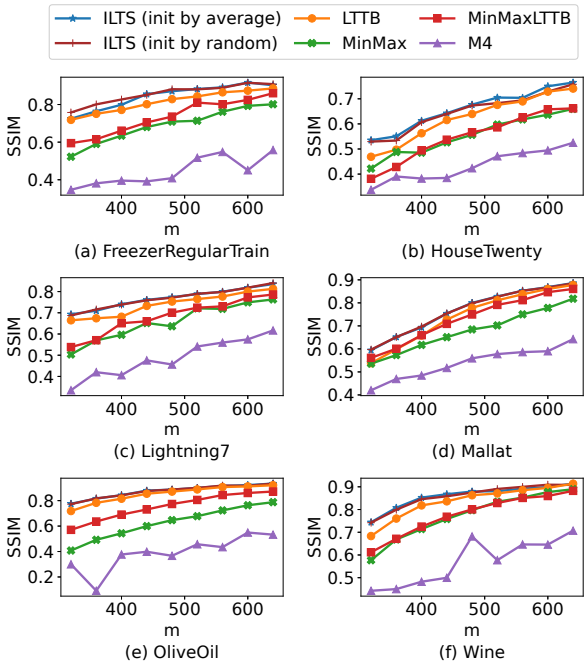

Figure 20: SSIM comparison experiments (adding ILTS initialized by random points)

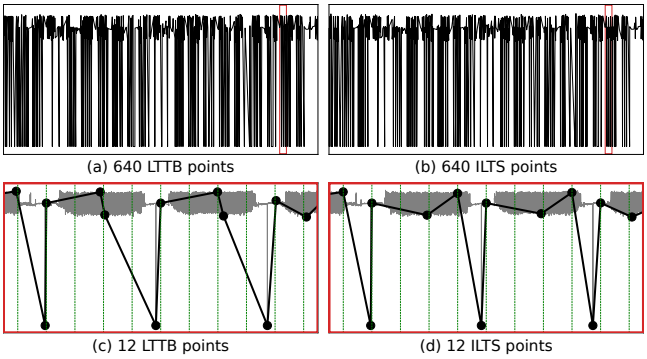

Figure 21: LTTB v.s. ILTS. The gray lines in (c) and (d) represent the original time series. ILTS visually captures the dense area more effectively through iterations.

on ILTS initialized by either average or random points in Figure 20. As can be seen, ILTS works well under both average and random initialization.

A.8 Better Figure 1 and 2

To better illustrate the motivation behind ILTS using iterations, we add Figure 21 and Figure 22 as supplementary to Figure 1 and Figure 2, respectively. The new examples demonstrate the superiority of ILTS in representing visually dense areas.

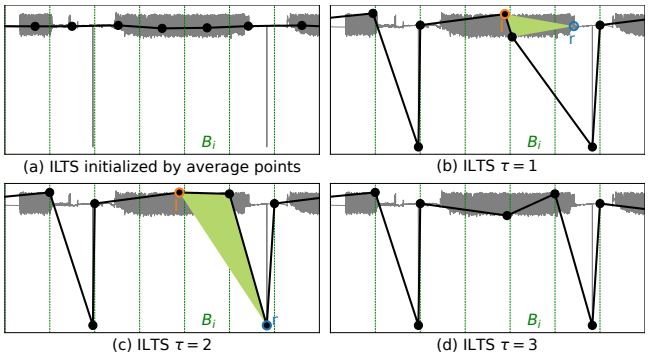

Figure 22: ILTS iteration example (continue Figure 21)

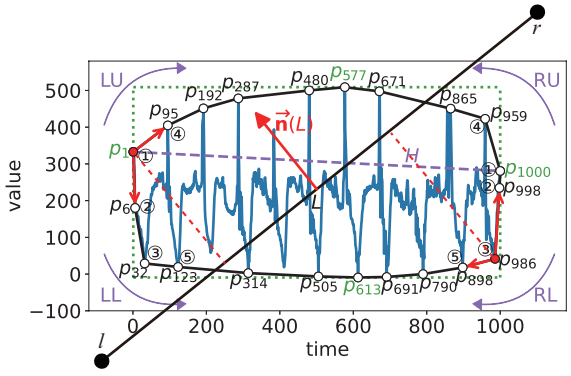

LU={p6,p1},LL={p1,p6},RU={p998,p1000},RL={p1000,p998}

LU={p6,p1},LL={p1,**p6**,p32},RU={p998,p1000},RL={p1000,**p998**,p986}

LU={p6,**p1**,p95},LL={p1,p6,p32},RU={p998,**p1000**,p959},RL={p1000,p998,p986}

LU={p6,**p1**,p95},LL={p6,**p32**,p123},RU={p998,p1000,p959},RL={p998,**p986**,p898}

Figure 23: Improved example of the convex hull acceleration (for better Figure 4)

A.9 Better Figure 4

We improve the original Figure 4 in Figure 23. The fixed line L is shown to connect the two heuristic points l and r. The effect of normal vector is emphasized by adding auxiliary perpendicular lines. The intermediate results of triplets LU, LL, RU, RL during fast search on the convex hull are also labeled in the figure.

A.10 Experiments on More Datasets

We add experiments on two large-scale real datasets. **Stock** is an open stock market data on Kaggle [https://www.kaggle.com/datasets/debashis74017/stock-market-data-nifty-100-stocks-5-min-data]. The largest input number used in our experiments is $n = 312,960,350$. **Train** is a train sensor dataset provided by real customers of Apache IoTDB. The largest input number used in our experiments is $n = 306,726,888$. The experimental results in Figure 24 show that ILTS achieves the best visualization efficacy, and its query latency increases linearly with the number of sampled points m, and sublinearly with the number of input points n. Note that the query efficiency advantage of ILTS becomes more apparent on a larger n. This is because as n increases, the percentage of disk

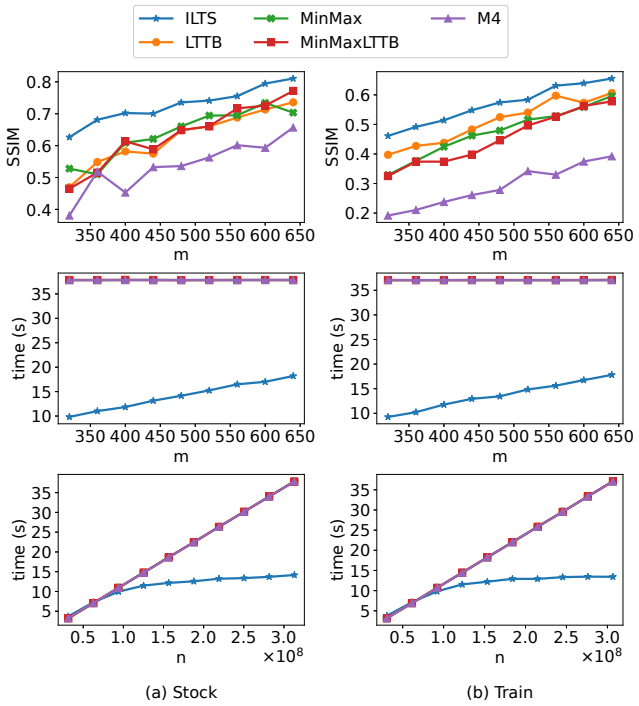

Figure 24: Experiments on two additional datasets

pages pruned by the upper bounding technique (Section 4.3) also increases.

Algorithm 3: Iterative largest triangle sampling (augmented with redundancy removal)

Input: an input time series $T = \{p_1, \ldots, p_n\}$, a threshold m for the length of the sampled time series, the number of iterations τ

Output: a sampled time series $ILTS(T) = \{q_1^*, \ldots, q_m^*\}$

determine all time buckets B_i, $i = 1, \ldots, m$, as in Definition 2
initialize q_i^* by either a random sample or the average of all points in the bucket B_i, $i = 1, \ldots, m$
initialize the flag array R with the first $m-1$ elements being *false* and the last element being *true*
for $k \in \{1, \ldots, \tau\}$ **do**
  initialize the flags $allEq = true$, $leftEq = true$
  for $i \in \{2, \ldots, m-1\}$ **do**
    if $leftEq$ ***and*** R_{i+1} **then**
      set $R_i = true$
      continue
    set $l = q_{i-1}^*$, $r = q_{i+1}^*$, $q = q_i^*$
    set $q_i^* = \arg\max_{p \in T,\, p.t \in B_i} \triangle lpr$ by the largest triangle routine as in Definition 3, with convex hull acceleration
    if $q_i^* = q$ **then**
      set $leftEq = true$, $R_i = true$
    else
      set $allEq = false$, $leftEq = false$, $R_i = false$
  if $allEq$ **then**
    break
return $\{q_1^*, \ldots, q_m^*\}$